UC Davis
UC Davis Previously Published Works

Title

Nitrogen Fate During Agricultural Managed Aquifer Recharge: Linking Plant Response, Hydrologic, and Geochemical Processes

Permalink

https://escholarship.org/uc/item/11d3475j

Authors

Dahlke, Helen E
Levintal, Elad
Huang, Laibin
et al.

Publication Date

2022

DOI

10.2139/ssrn.4252489

Peer reviewed

1   **Nitrogen fate during agricultural managed aquifer recharge: linking plant**

2   **response, hydrologic, and geochemical processes**

3   Elad Levintal[1], Laibin Huang[1], Cristina Prieto García[1], Adolfo Coyotl[1], Matthew

4   W. Fidelibus[2], William R. Horwath[1], Jorge L. Mazza Rodrigues[1,3], Helen E.

5   Dahlke[1,*]

6   1. Department of Land, Air and Water Resources, University of California, Davis, CA 95616, USA

7   2. Department of Viticulture and Enology, University of California, Davis, 1 Shields Ave., Davis, CA 95616, USA

8   3. Environmental Genomics and Systems Biology Division, Lawrence Berkeley National Laboratory, Berkeley, CA

9   94720, USA

10

11   * Corresponding author. E-mail address: hdahlke@ucdavis.edu (H.E. Dahlke)

12   **Abstract**

13   Agricultural managed aquifer recharge (Ag-MAR, on-farm recharge), where farmland is

14   flooded with excess surface water to intentionally recharge groundwater, has received increasing

15   attention by policy makers and researchers in recent years. However, there remain concerns

16   about the potential for Ag-MAR to exacerbate nitrate (NO_3^-) contamination of groundwater, and

17   additional risks, such as greenhouse gas emissions and crop tolerance to prolonged flooding.

18   Here, we conducted a large-scale, replicated winter groundwater recharge experiment to quantify

19   the effect of Ag-MAR on soil N biogeochemical transformations, potential NO_3^- leaching to

20   groundwater, soil physico-chemical conditions, and crop yield. The field experiment was

21   conducted in two grapevine vineyards in the Central Valley of California, which were each

22   flooded for 2 weeks and 4 weeks, respectively, with 1.31 and 1.32 m^3 m^{-2} of water. Hydrologic,

23   geochemical, and microbial results indicate that NO_3^- leaching from the first 1 m of the vadose

24   zone was the dominant N loss pathway during flooding. Based on pore water sample and N_2O

25   emission data denitrification played a lesser role in decreasing NO_3^- in the root zone but

26   prolonged anoxic conditions resulted in a significant 29% yield decrease in the 4-week flooded

27   vineyard. The results from this research, combined with data from previous studies, are

28   summarized in a new conceptual model for integrated water-N dynamics under Ag-MAR. The

29   proposed model can be used to determine best Ag-MAR management practices.

31   **1.   Introduction**

32   One-quarter of the world's population and 40% of agricultural production relies on overdrafted

33   groundwater sources (Connor, 2015), with an expected increase in groundwater reliance due to

34   climate change and growing water demand (Gorelick and Zheng, 2015; Haddeland et al., 2014;

35   Siebert et al., 2010; Wada et al., 2010). Thus, reducing pressure on overdrafted groundwater

36   systems is crucial to increase global resilience of food and drinking water in response to growing

37   human population and climate change pressures.

38   Agricultural managed aquifer recharge (Ag-MAR, or on-farm recharge) is a form of managed

39   aquifer recharge (MAR) where farmland is flooded with excess surface water to recharge

40   groundwater intentionally (Grinshpan et al., 2021; Kocis and Dahlke, 2017; Waterhouse et al.,

41   2020) and it has been increasingly used across the globe to address groundwater overdraft

42   (Dillon et al., 2019; Levintal et al., 2022). The purpose of Ag-MAR, in comparison to more

43   traditional MAR methods, is to transfer large amounts of surplus surface water from rivers or

44   reservoirs to agricultural land (e.g., idle land, agricultural fields and orchards) that serve as

45   spreading grounds for the recharge (Dahlke et al., 2018).

46   Ag-MAR adoption has increased in recent years, particularly in the USA and Europe

47   (Grinshpan et al., 2021; Negri et al., 2020; Niswonger et al., 2017). In California, for example,

48   Ag-MAR is implemented as one of the methods to overcome ongoing groundwater depletion

49   (Kocis and Dahlke, 2017). However, using farmland as spreading grounds bears the risk to leach

50   contaminants from the water or soil to groundwater which can impact drinking water quality

51   (Bachand et al., 2014), waterlogging of the root zone for long periods that can reduce crop health

4

52   (Ganot and Dahlke, 2021a), and ecosystem service tradeoffs, such as short and long-term effects

53   on in-stream flows (Levintal et al., 2022). Out of the above, leaching of legacy nitrogen (N),

54   mainly in the form of nitrate (NO_3^-), is possibly the most widespread environmental risk of Ag-

55   MAR. Consumption of drinking water above the maximum contaminant level (MCL; 10 mg L^{-1}

56   NO_3^--N in California) can increase the risk of cancers, birth defects, and other adverse health

57   effects (Weitzman et al., 2022). Globally, nitrate is the primary nonpoint source pollutant of

58   groundwater (Beganskas et al., 2018; Bishayee et al., 2022; Richa et al., 2022), whereby

59   agricultural lands serve as the main source for NO_3^- due to the buildup of legacy NO_3^- resulting

60   from years of fertilizer use inefficiencies (Van Meter et al., 2016; Waterhouse et al., 2020).

61   In comparison to the deep vadose zone, NO_3^- concentrations are highest either in the topsoil (0-

62   10 cm) or just below the root zone (~1-2 m) where NO_3^- is transported out of reach of roots with

63   irrigation (Waterhouse et al., 2021, 2020). NO_3^- in soils can originate from N-based fertilizer or

64   from N transformations, such as nitrification of ammonium (NH_4^+)-based fertilizer or nitrification

65   of NH_4^+ from mineralized soil organic-N (Stein and Klotz, 2016). In contrast, NO_3^- removal

66   pathways are denitrification and immobilization (controlled by microbial activity), leaching

67   (controlled by infiltration rate), and plant uptake (Kurtzman et al., 2021; Long et al., 2013;

68   Schmidt et al., 2011; Zhang et al., 2018). The governing processes during Ag-MAR are NO_3^-

69   leaching, mineralization, nitrification, and denitrification (Murphy et al., 2021; Schmidt et al.,

70   2012; Waterhouse et al., 2021). The latter is favored under suboxic to anoxic conditions, as

71   expected during soil saturation of Ag-MAR events (Ganot and Dahlke, 2021b). N transformation

72   processes, excluding leaching, occur in the soil dependent on electron donor availability (e.g.,

73   dissolved organic carbon (DOC)) and microbial community abundance and composition

74   (Peterson et al., 2013; Scarlett et al., 2021). Ambient conditions may also influence NO_3^-

75   transformations, including soil moisture, carbon/nitrogen ratio, pH, soil texture, temperature,

76   vegetation, oxidation-reduction potential (ORP), and water residence time in the topsoil (Kraft et

77   al., 2014; Stein and Klotz, 2016). The underlying assumption adopted by previous researchers is

78   that NO_3^--related processes are negligible below the root zone; therefore, NO_3^- leached below the

79   root zone will eventually reach the groundwater (Baram et al., 2016b; Gurevich et al., 2021).

80   Thus, in Ag-MAR, the aim is to reduce legacy NO_3^- via denitrification before NO_3^- leaching

81   occurs below the root zone.

82   NO_3^- leaching is an environmental risk that is not unique to Ag-MAR, but can occur in any

83   MAR method (e.g., infiltration basins; Beganskas et al., 2018), since it mainly depends on the

84   source of NO_3^- in the recharge environment. For example, Beganskas et al. (2018), Gorski et al.

85   (2019), and Schmidt et al. (2011) recharged stormwater runoff from upslope agricultural fields in

86   an infiltration basin in the Pajaro Valley, California, which contained 22-25 mg L^{-1} NO_3^--N. If

87   low-N source water is used in Ag-MAR (e.g., mountain runoff or snowmelt), elevated NO_3^- in

88   soil pore water often originates from the soil matrix from recurring fertilizer applications.

89   Only a few studies exist to date that have estimated soil NO_3^- biogeochemical transformations

90   and NO_3^- leaching under Ag-MAR. As one of the first, Bachand et al. (2014) investigated NO_3^-

91   fate in a large farm-scale experiment where they flooded alfalfa, wine grapes, tomatoes, and

92   fallow land for various periods ranging from 10 days to one month. They proposed a general

93   framework for NO_3^- fate under Ag-MAR, concluding that NO_3^- will be leached to groundwater,

94   but pore water and groundwater NO_3^- concentrations will be diluted following consecutive flood

95   applications (assuming the use of low-NO_3^- water). However, they did not investigate any N

96 transformations. Waterhouse et al. (2020) estimated the potential risk of NO_3^- leaching under Ag-

97 MAR using only data from 10 m deep soil cores from 12 fields (no flooding was performed),

98 focusing on three crops (almonds, processing tomatoes, and wine grapes) and two soil groups

99 (low- and high-infiltrating soils). They concluded that vineyards were the most suitable crop for

100 Ag-MAR due to low legacy NO_3^- resulting from the crop's deep roots and overall low N inputs.

101 Murphy et al. (2021) investigated the role of flooding frequency (i.e., three flooding events of

102 0.15 m depth each) and soil texture on N dynamics and potential NO_3^- leaching in laboratory

103 column experiments. Each flooding event was on the scale of hours followed by a drying period

104 of several days to two weeks. They observed that the majority of initially present soil NO_3^-

105 leached during the first few hours of the first water application when conditions for

106 denitrification (i.e., removal of NO_3^-) were unfavorable due to oxic conditions. NO_3^- leaching was

107 quantified only for the laboratory column experiments ranging between 0.028 and 0.072 g NO_3^--

108 N m^{-2} for every 1 cm^3 cm^{-2} of applied water. Based on the combination of lab assay and field data

109 Murphy et al. (2021) showed that using only soil core data from pre- and post-flooding is

110 insufficient to quantify NO_3^- leaching, emphasizing the need for continuous field measurements

111 during Ag-MAR.

112 In a recent modeling study, Waterhouse et al. (2021) investigated Ag-MAR effects on

113 denitrification rates and NO_3^- leaching in a heterogeneous, layered deep vadose zone (~15 m).

114 They found that denitrification rates were highest in response to one continuous extensive water

115 application due to the development of suboxic conditions compared to small incremental

116 recharge events. However, this continuous water application scenario also leached NO_3^- deeper

117 into the vadose zone. None of the above studies measured N-related biogeochemical processes

118 during continuous, long (e.g., several weeks) flooding applications for Ag-MAR in different

119 soils. This suggests that understanding of N fate and NO_3^- leaching at the field scale is still

120 elusive in Ag-MAR; thus, further research is needed.

121   This study aims to investigate the environmental impacts of Ag-MAR using a large-scale field

122 experiment conducted in the Central Valley, California (semiarid Mediterranean climate). Two

123 vineyards, each with a different soil texture, were simultaneously flooded during late winter, one

124 for four weeks (V1) and the other for two weeks (V2). Combining hydrologic, geochemical, and

125 microbial process analyses, we quantified the effects of Ag-MAR on the soil N biogeochemical

126 transformations, potential NO_3^- leaching to groundwater, soil physico-chemical conditions, and

127 crop response. The results from this research, combined with data from previous studies, are

128 summarized in a new conceptual model for integrated water-N dynamics.

129 **2.**   **Materials and Methods**

130 *2.1.*   *Description of site, water application, and measurements*

131   A replicated field experiment was conducted at the Kearney Agricultural Research and

132 Extension Center (http://kare.ucanr.edu/) located 20 km southeast of the city of Fresno in the

133 Central Valley of California, USA. Two mature (>40-year-old) own-rooted 'Thompson Seedless'

134 grapevine (*Vitis vinifera* L.) vineyards were flooded; the first vineyard for four weeks (V1) and

135 the second vineyard for two weeks (V2) (February–March 2020). V1 is on a very deep fine

136 sandy loam (*Hesperia,* coarse-loamy, mixed, nonacid, thermic Xeric Torriorthents) with a

137 saturated hydraulic conductivity (K_{sat}) of 0.02 m hr^{-1} for the first 1 m depth (USDA-NCSS soil

138 survey data), and V2 is on a fine sandy loam (*Hanford*) with a K_{sat} of 0.1 m hr^{-1} for the first 1 m

139   depth. Using a randomized complete block design, each vineyard was divided into six individual

140   subplots, of which three were artificially flooded and three were kept under the natural

141   precipitation regime (i.e., control) (**Fig. 1a**). Individual subplots were separated from one another

142   using berms approximately 0.5 m high and 0.8 m wide (see **Fig. 1b**). The groundwater table was

143   ~23 m below the surface measured in October 2019. The site has a semiarid, Mediterranean

144   climate (Onsoy et al., 2005). Mean air temperature and total precipitation during the flooding

145   period was 21.9 °C and 0.03 m, respectively.

146   Flooding started automatically at 06:00, 14:00, and 22:00 for 2-3 hrs at both vineyards each day,

147   except for the first four days during which manual operation was used to adjust flow rates to

148   prevent overflow to adjacent fields. Flooding of the vineyards started on 02/25/2020 and ended

149   on 03/10/2020 (V2) and 03/24/2020 (V1). Two flow meters were used at the water inlet point of

150   each vineyard to measure total applied water. Flooding was done using a single water outlet

151   located at the west side of each row within the flooded subplots. A total of 7298 and 4659 m^3

152   were discharged at V1 and V2, respectively. Commonly Ag-MAR would be conducted using

153   surface water. However, due to drought during the winter of 2019-2020 no surface water was

154   available at our experimental site, therefore, pumped groundwater was used as an alternative

155   water source for Ag-MAR. Groundwater was determined as a suitable alternative to surface

156   water because N species concentrations in groundwater were found to be comparable to those of

157   surface water in this area, as previously reported by Bachand et al. (2014).

158   Ten monitoring profiles were instrumented for continuous measurements, five within each

159   vineyard (**Fig. 1a**). Out of the five profiles in each vineyard, only one profile was installed in the

160   control (i.e., the non-flooded subplots) to allow higher spatial measurement resolution in the Ag-

161   MAR treatment subplots, which are the focus of this study. Each profile was installed 0.7 m from

162   the vine row toward the furrow and included three sensor clusters at 0.2, 0.6 and 1 m depth. Each

163   cluster included measurements of soil moisture and temperature (TEROS12, Meter, WA, USA),

164   O_2 in gaseous phase (KE-25, Figaro, Japan), and ORP using constructed platinum electrodes

165   (following Owens et al., 2005) and commercial Ag/AgCl reference electrodes (Accumet, Thermo

166   Fisher Scientific, MA, USA). Additional measurements included three pressure transducers

167   within stilling wells to record ponding levels (CS451, Campbell Scientific, UT, USA). Sensors

168   were placed in hand augered holes that were backfilled with soil while compacting it at

169   approximately 0.2 m intervals. Data were logged (CR1000 and CR800, Campbell Scientific, UT,

170   USA) at a 10-min interval. The complete site and sensor descriptions are detailed in **Figs. 1a** and

171   **1c**, respectively, and a photo taken during the flooding is presented in **Fig. 1b**. Atmospheric

172   measurements (temperature, precipitation) at 60-min intervals were taken from the California

173   Irrigation Management Information System station (CIMIS; station 39 Parlier, CA) situated 400

174   m from the experimental site.

175   Crop management practices followed standard recommendations with grape harvest in

176   September and cane pruning on 20 January 2020. Both vineyards were fertilized once per year,

177   two months after the flooding (end of April 2020), when 336 kg ha^{-1} of N fertilizer (ammonium

178   sulfate 21-0-0 with 24% sulfur) were applied. Vines were manually harvested on 23 September

179   2020. The entire amount of fruit harvested from each plot was recorded and used for statistical

180   analyses.

181
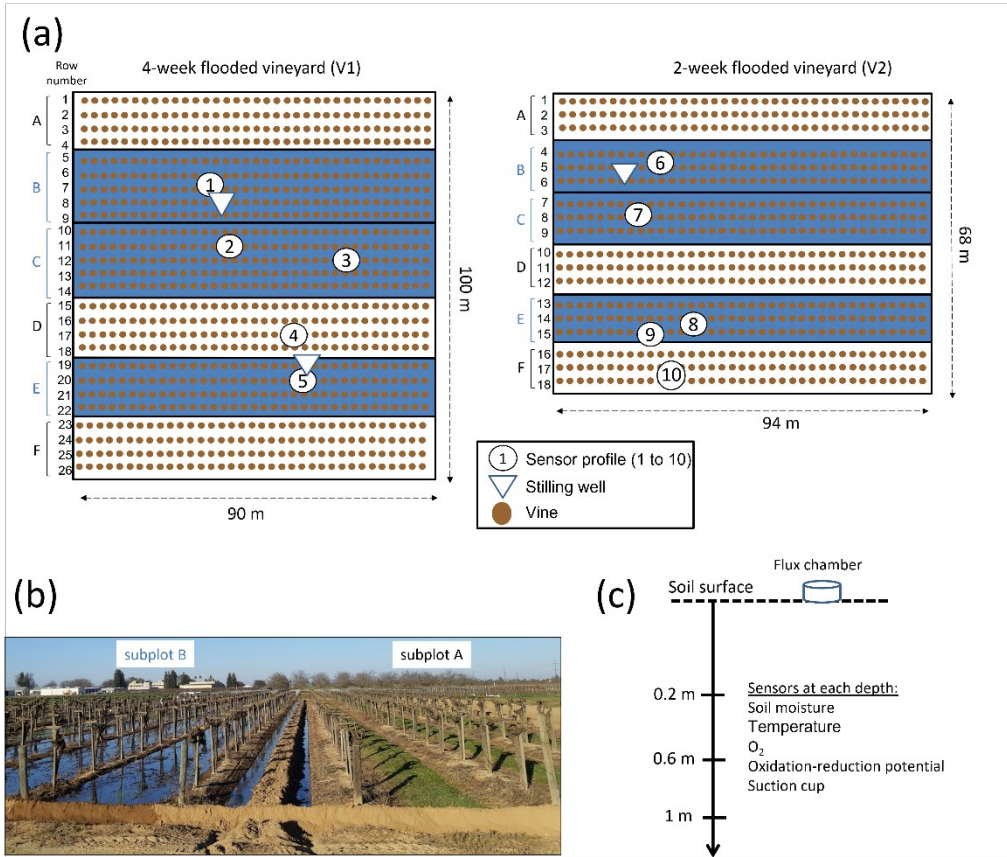
Fig. 1. Experimental setup. (a) Sensor locations in each vineyard. Flooded subplots are marked in blue. (b) A photo of the 4-week flooded vineyard (V1) showing subplots A and B during the flooding. (c) Sensor locations within a single profile.

2.2.   Pore water, gas emission, and soil sampling

Pore water, greenhouse gas (GHG) emission, and soil sampling campaigns were carried out to better understand and quantify the N biogeochemical processes within the soil. Pore water samples were taken using suction cups (LT-DBL, Irrometer, CA, USA), installed at each of the ten profiles and at the same depths as the sensor clusters (0.2, 0.6, and 1 m). After installation, suction cup boreholes were backfilled with sieved soil slurry, followed by 0.15 m of soil, and sealed with 0.05 m bentonite; shallow 0.2 m suction cups were installed without bentonite. Pore

192   water was sampled on average twice a week during the flooding period and once a week at other

193   times, except for one continuous 5-day measurement campaign after fertilization to capture the

194   fertilization effect on N processes. Samples were stored on ice until storage in a 4 °C cold room.

195   Pore water was analyzed for NO_3^-, NH_4^+, and DOC. Analytical protocols are detailed in the

196   supporting information.

197   *In-situ* GHG emissions were measured using the closed-flux vented chamber method (e.g.,

198   Garland et al., 2014). Twenty individual chambers were installed, each made from 0.26 m

199   diameter polyvinyl chloride (PVC) pipe, consisting of a bottom ring and a cap. Two chambers

200   were installed near each of the ten sensor profiles shown in **Fig. 1a** – one on the mount between

201   the vines and one in the furrow. Collars were inserted into the soil to a depth of 0.07 m and left

202   in the same location for the entire duration of the experiment. Chamber headspace was measured

203   after each sampling to account for any reduction in volume due to water within the chamber. At

204   sampling time, the chambers were sealed onto the collars with a rubber sleeve made from a tire

205   innertube. Gas samples were taken through a rubber septum at four times (0, 30, 60, and 80 min)

206   using a 20 mL air-tight syringe and injected into pre-evacuated 12 mL vials. Before each

207   sampling effort, a 12V fan (installed within each chamber) was activated for 20-30 seconds to

208   ensure a mixed representative headspace sample. Temperature was measured during each time

209   step in 10 out of the 20 chambers. Samples were analyzed using a gas chromatograph (Shimadzu

210   Trace Gas GC, Shimadzu Corp., Kyoto, Japan) for carbon dioxide (CO_2), methane (CH_4), and

211   nitrous oxide (N_2O). Fluxes were calculated according to Garland et al. (2011). Gas samples

212   were taken on similar days as the water samples and mostly around noon.

213   Soil samples were taken from four depths: 0-0.1, 0.1-0.2, 0.5-0.6, 0.8-1 m using a hand auger.

214   All samples were taken from the same rows in which the sensor profiles were installed and at

215   similar distances from the vines toward the furrow ($\sim$0.7 m). Samples were stored identical to

216   pore water samples and taken during four campaigns according to the different experimental

217   stages: 02/06/2020 (baseline data), 03/10/2020 (end of flooding at V2), 03/25/2020 (end of

218   flooding at V1, and two weeks post-flooding at V2), and 04/15/2020 (three weeks post-flooding

219   at V1). Soil samples were analyzed for NO_3^-, NH_4^+, DOC, and texture. In addition, soil

220   subsamples were stored at -80 °C and later used for incubation experiments (see details in

221   section 2.4).

222   *2.3.*   *Nitrogen leaching estimates*

223   The amount of NO_3^- leaching below 1 m (the root zone in the case of flooded-irrigated

224   vineyards) during flooding was quantified using a vadose-zone-based water and N mass balance

225   model (Baram et al., 2016b), in which M_A is the cumulative mass of NO_3^- per flooded area (as

226   NO_3^--N [g m^{-2}]) lost through leaching (**Eq. 1**) and M is the total mass of NO_3^- (as NO_3^--N [g]) lost

227   during the flooding (**Eq. 2**):

228 $$M_A = \sum_{i=1}^{n} L_i C_i \Delta t_i \tag{1}$$

229 $$M = \sum_{i=1}^{n} M_{A_i} A \tag{2}$$

230   where L is the amount of water leaching below 1 m estimated using the infiltration rate (section

231   2.5) [m d^{-1}], C is the average NO_3^--N concentration in the leaching water at 1 m depth [g m^{-3}], Δt

232   is a given time period [d] between each ith measurement, and A is the flooded surface area [m^2].

13

233 Because all pore water NH_4^+ samples measurements at both vineyards were < 1 g m^{-3}, these

234 values were considered negligible in the quantification of total inorganic N leached for modeling

235 purposes.

236 *2.4.   Potential denitrification*

237   Incubation experiments were conducted in the lab to assess denitrification rates during the

238 flooding period. Net denitrification rates were estimated using a modified method of Petersen et

239 al. (2012). Briefly, field-moist soil (15 g) collected one day before flooding and one day after

240 flooding was added to 100 ml serum bottle and sealed with rubber stopper and metal caps, and

241 then flushed with N_2 gas for 10 min to create anaerobic conditions and afterwards equilibrated

242 with atmospheric pressure using a syringe. Bottles were placed in an incubator for 7 days at

243 25°C. Incubated samples were analyzed for changes in NO_3^- concentrations on the initial and 7th

244 day to determine denitrification rates.

245 *2.5.   Hydrological analysis*

246   Daily infiltration rates were calculated using two independent methods. In the first method, the

247 total applied water was divided by the flooded surface area and total number of flooding days for

248 each vineyard. The second method, also referred to as the falling head method, estimates the

249 infiltration rate from the slope of the decreasing ponding level in each flood plot after water shut-

250 off, which is then normalized for daily infiltration rates. Both methods provide bulk infiltration

251 rates.

252   Groundwater recharge was calculated using a one-dimensional vertical water balance model

253 (**Eq. 1**) (Dahlke et al., 2018). A single solution was solved for each of the eight flooded

254 monitoring profiles using input data averaged over an hourly interval. The fraction of applied

255 water going to deep percolation towards the groundwater table was calculated by accounting for

256 evapotranspiration and storage in pore space.

257 $$R_t = I_t + P_t - ET_t - \Delta S_t - Q_t \tag{3}$$

258 where R_t [m] is recharge, I_t [m] is the amount of applied surface water, P_t [m] is precipitation,

259 ET_t [m] is evapotranspiration, ΔS_t [m] is the change in soil storage, and Q_t [m] is surface runoff at

260 time step t, which was assume to be negligible due to the use of berms. **Eq. 3** was solved using

261 the Thornthwaite-Mather procedure (Steenhuis and Molen, 1986) performed via Excel solver

262 (Office 365 ProPlus, 2020). This procedure was used in previous Ag-MAR studies (Dahlke et al.

263 2018). The procedure was solved for the first meter assuming this is also the maximum depth of

264 the major root zone (Araujo et al., 1995) in which evapotranspiration demand takes place.

265 **3.   Results**

266 *3.1.   Recharge and soil physical characteristics*

267 The flood treatments in the two vineyards showed different hydrologic and biogeochemical

268 responses during and after the flooding for recharge (V1 - **Fig. 2** and V2 – **Fig. 3**). As a result of

269 field topography, flooding was not uniform in the flooded subplots. Dry areas occurred in the

270 eastern part of V1 (**Fig. 1a**; subplot C) and V2 (**Fig. 1a**; subplots C and E), effectively reducing

271 the flooded area to an average of 4613 m² (90%) and 3035 m² (75%) in V1 and V2, respectively.

272 Soil ORP and O_2 concentration decreased rapidly in V1, reaching anoxic conditions (ORP < 100

273 Eh) at 0.2, 0.6 and 1 m depth 1-3 days after flooding started (**Figs. 2c** and **2d**). Reducing, anoxic

274 conditions were sustained for 12-18 days after flooding ended, leading to ~40 days of continuous

275 reducing conditions within the soil profile in V1. In contrast to V1, V2 maintained good aeration

276 during the flooding and only experienced anoxic conditions at the shallowest depth of 0.2 m and

277 for a short duration (2-5 days) (**Figs. 3c** and **3d**). O_2 and ORP averaged ~20% O_2 and ~400 Eh

278 ORP at all other depths within the flooded soil profiles in V2. Although flooded plots at both

279 vineyards reached near or fully saturated conditions as indicated by the soil moisture (**Figs. 2b**

280 and **3b**), the observed differences in soil O_2 and ORP clearly indicate different environmental

281 conditions that impacted biogeochemical processes in each vineyard.

282 As expected, control plots of both vineyards showed predominantly oxic ORP conditions (i.e.,

283 O_2 ~20% and ORP > 500 Eh) for the duration of the experiment and only abrupt soil moisture

284 increases after rain events. The only exception was profile 4 in V1 (see **Fig. 1a** for location),

285 which showed a soil moisture increase at 1 m depth followed by a decrease in O_2. Since no soil

286 moisture increase was observed at 0.2 and 0.6 m, we attributed this change to the possibility of

287 lateral flow from the flooded subplots, impacting the oxygen status in the deeper soil profile.

288
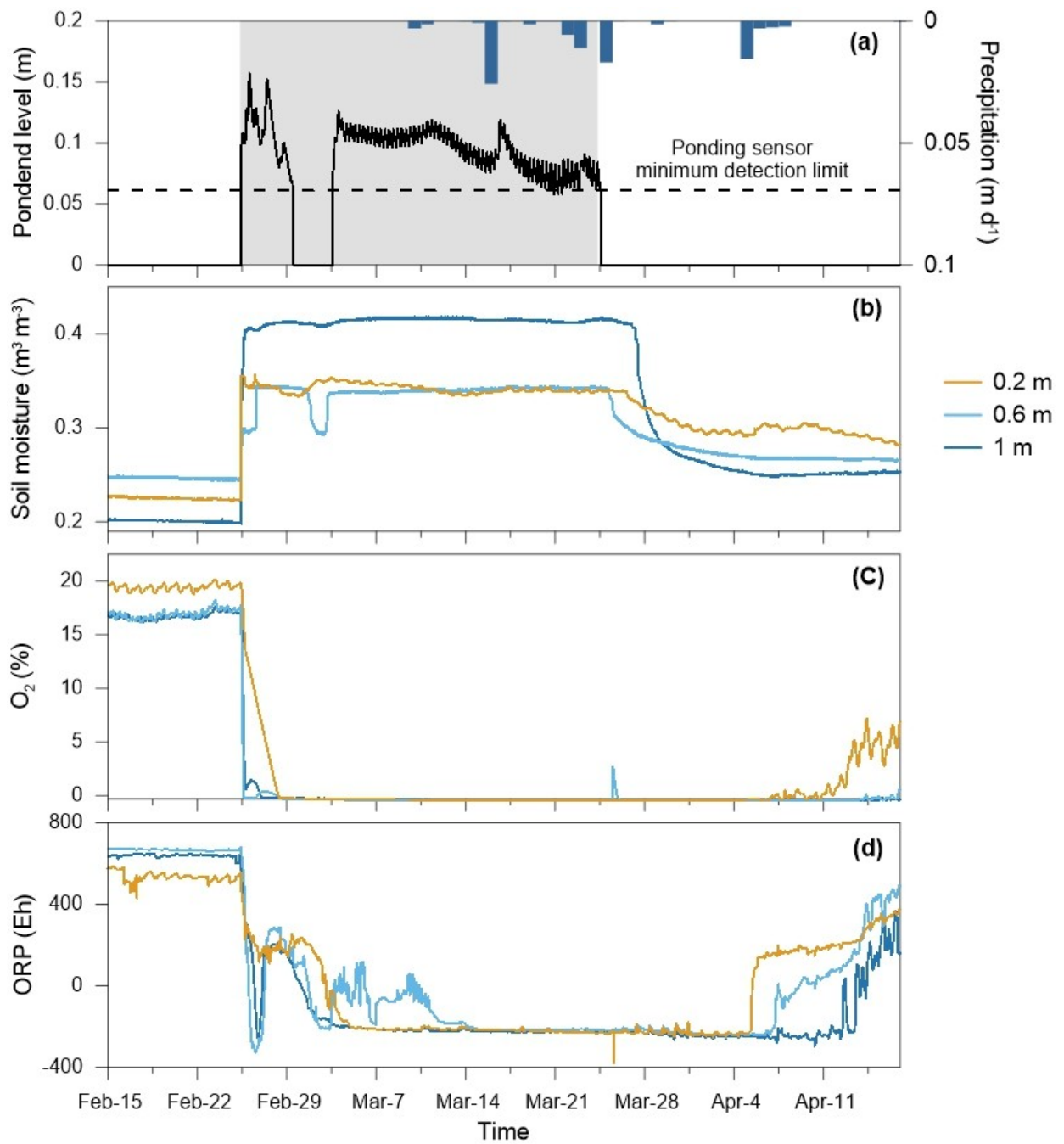
Fig. 2. Time series data for the 4-week flooded vineyard (V1) for selected hydrologic and physico-chemical parameters from profile 1 (see **Fig. 1a** for profiles location). ORP – oxidation-reduction potential. The gray shaded area in (a) shows the time of water application. Blue

precipitation bars show the daily totals taken from a meteorological station located 400 m from

the experimental site.

294
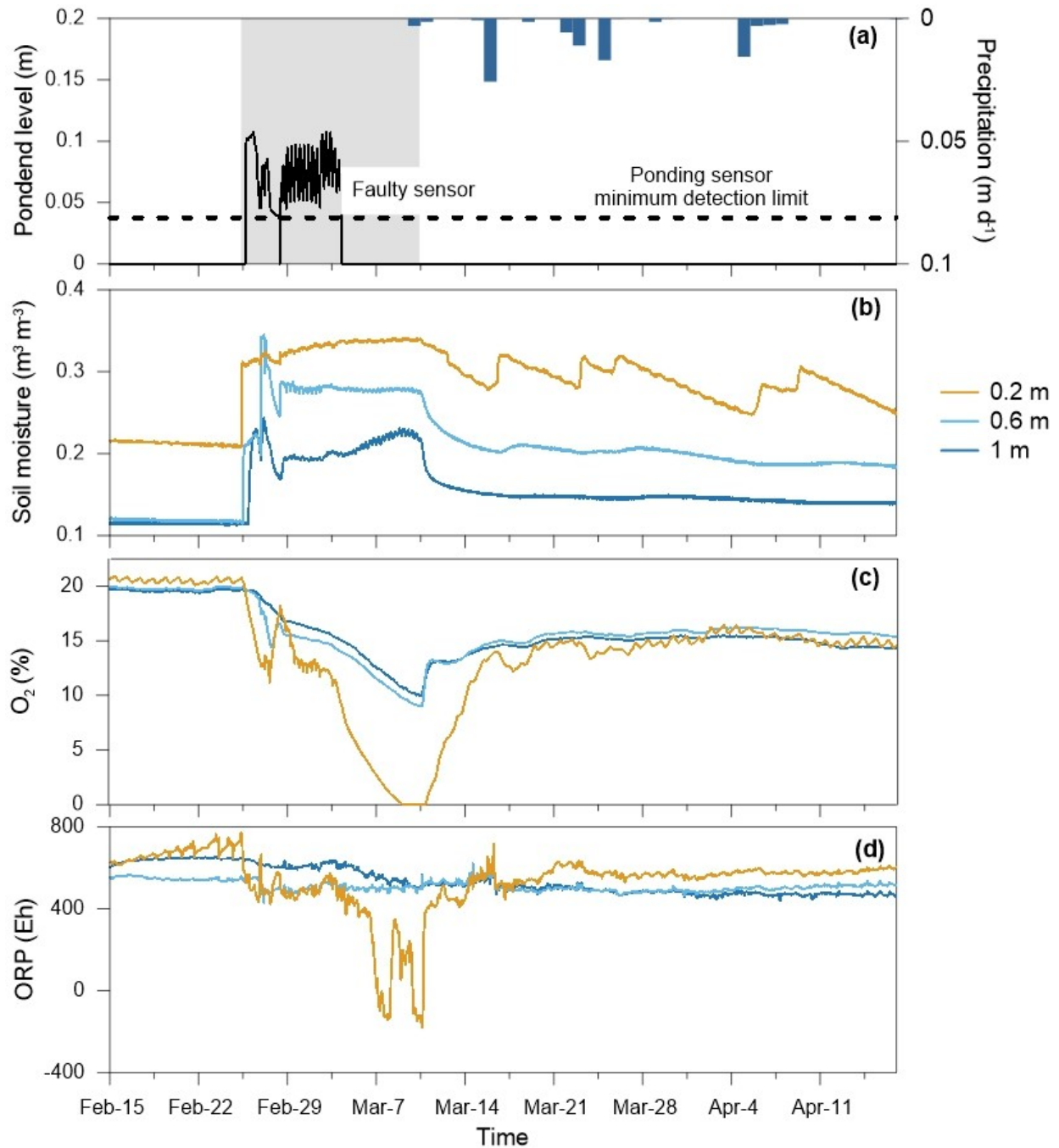
Fig. 3. Time series data for the 2-week flooded vineyard (V2) for selected hydrologic and

physico-chemical parameters from profile 7 (see **Fig. 1a** for profiles location). ORP – oxidation-

297 reduction potential. Gray shaded area represents the flooding duration. Blue bars in plot a show

298 daily precipitation totals.

299 *3.2. Infiltration rates and recharge*

300 The experimental site received little precipitation prior and during the experiment (**Fig. 2a**), thus

301 providing an opportunity to study infiltration processes and water balance changes associated

302 with Ag-MAR more closely. The infiltration rate in V1 was 0.088 ± 0.031 m d^{-1}. Estimated

303 groundwater recharge was $83\% \pm 1.2\%$ of the applied water using **Eq. 3**. The V2 site had a

304 higher infiltration rate of 0.171 ± 0.025 m d^{-1} with $86\% \pm 0.7\%$ of the applied water percolating

305 below 1 m. The higher V2 recharge rate is also reflected by the soil suitability ranking developed

306 by O'Geen et al. (2015) for California soils, which rates V2 as "excellent" for Ag-MAR whereas

307 the ranking of V1 is "moderately good" as supported by soil textural analysis, which showed a

308 higher sand fraction in V2 compared to V1 (**Fig. S1**). Upscaling the above values to each

309 vineyard indicates that 1.31 and 1.32 m^3 m^{-2} of water was recharged in the flooded areas in V1

310 and V2, respectively. Although V2 was only flooded for two weeks, the higher infiltration rate

311 (0.171 m d^{-1} in V2 compared to 0.088 m d^{-1} in V1) resulted in higher total recharge amounts.

312 *3.3. Pore water and residual soil chemistry*

313 Pore water NO_3^- and NH_4^+ data from both vineyards are presented in **Fig. 4**. During the first

314 week of flooding, NO_3^- concentrations in both vineyards decreased to zero at all three depths

315 (**Figs. 4b** and **4e**). Pore water NH_4^+ showed near-zero concentrations in the deeper soil profile

316 (0.6 and 1 m) before flooding and a clear reduction at 0.2 m depth (**Figs. 4c** and **4f**). DOC

317 concentrations in pore water remained approximately 20-60 mg DOC L^{-1} in both vineyards and

19

318 at all depths during flooding (**Figs. 4a** and **4d**). Nitrite (NO_2^-) was not measured directly and

319 assumed to be negligible following Bachand et al. (2014), which reported nitrite levels lower

320 than 0.1 mg NO_2^--N L^{-1} during their Ag-MAR study.
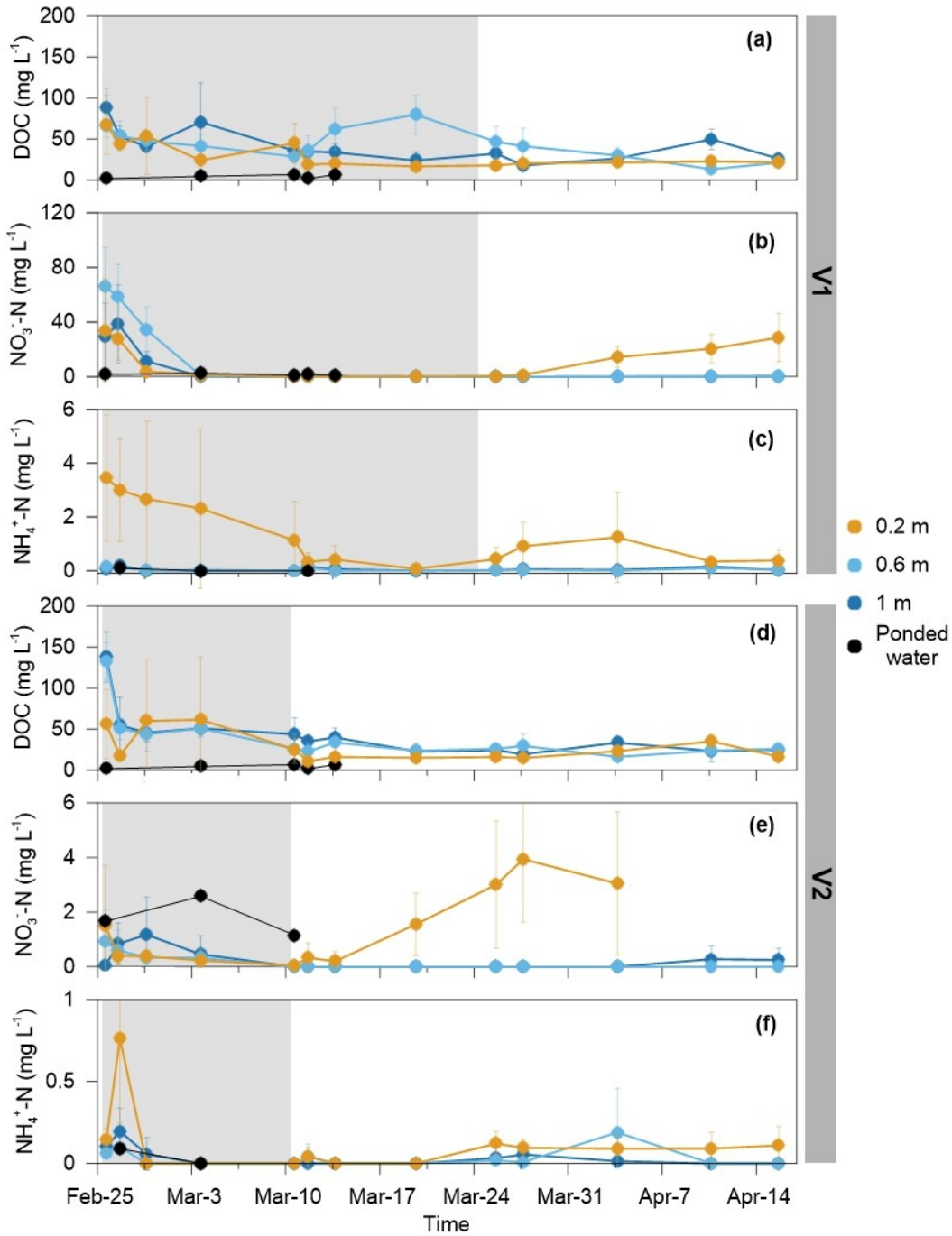
321

322 **Fig. 4**. Pore water results for the 4-week flooded vineyard (V1) (a-c) and the 2-week flooded

323 vineyard (V2) (d-f). Values are averages of the four flooded profiles in each vineyard with error

324 bars representing the standard deviation. Gray shaded areas represent the flooding duration.

325 Residual soil NH_4^+ in V1 depleted from 1-2 to near 0 mg NH_4^+-N kg^{-1} soil at all depths during

326 the flooding (**Fig. 5a**). In V2, pre-flooding NH_4^+ concentrations were already low (e.g., ~0 mg

327 NH_4^+-N kg $soil^{-1}$ below 0.1 m), with no significant change during flooding (**Figs. 5c** and **5d**).

328 Two weeks after the flooding ended, NH_4^+ levels in both vineyards increased uniformly at all

329 measured depths to ~1 and ~3 mg NH_4^+-N kg $soil^{-1}$ for V1 and V2, respectively (**Figs. 5a** and **5c**).

330 Similar post-flooding trends of increasing concentrations were also observed for NO_3^- in both

331 vineyards, however, only within the upper soil profile (0-0.2 m) where NO_3^- increased to 20-60

332 mg NO_3^--N kg^{-1} soil (**Figs. 5b** and **5d**).

333

21
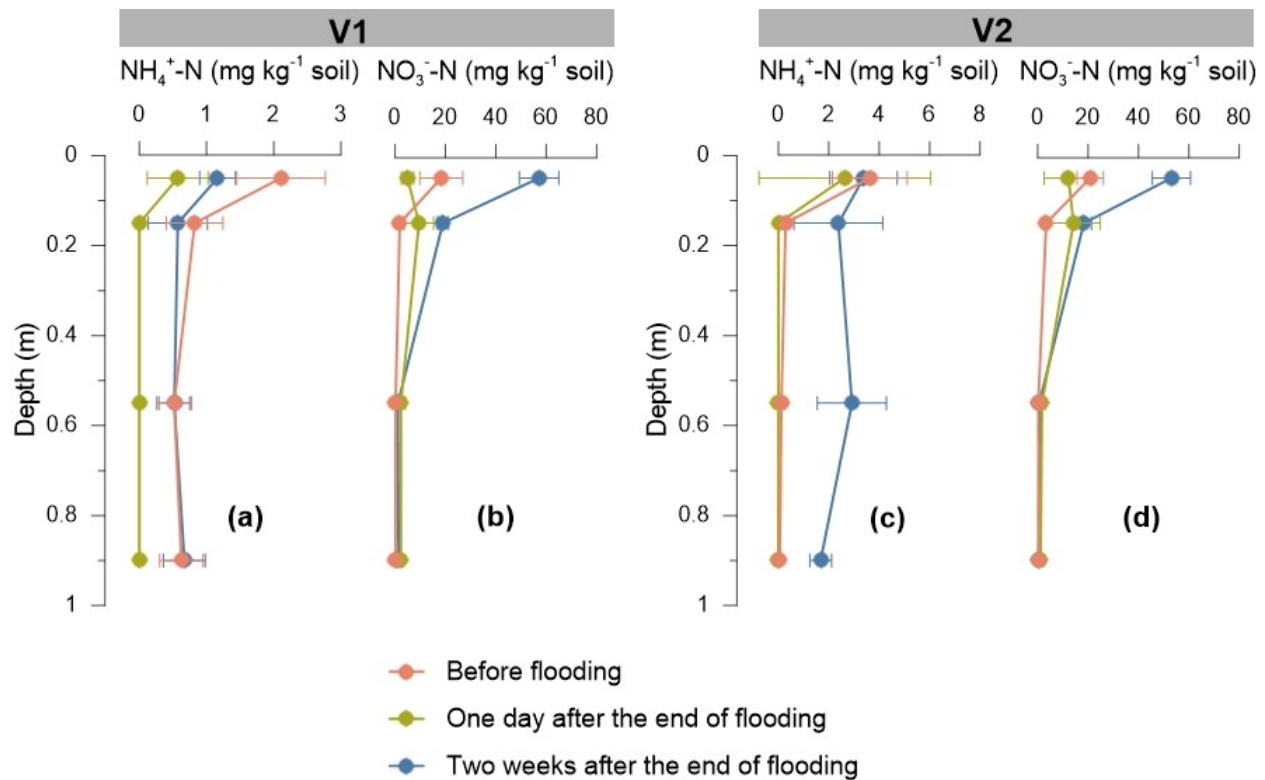
Fig. 5. Residual NO_3^- and NH_4^+ concentration in soil prior and after flooding for the 4-week flooded vineyard (V1) (a-b) and the 2-week flooded vineyard (V2) (c-d). Values are averages of the four flooded profiles in each vineyard with error bars representing the standard deviation.

3.4. Greenhouse gas emissions

During flooding, no changes in N_2O and CO_2 emissions were observed in the flood or control plots of V1 and V2 (**Fig. S2**). Post-flooding, N_2O emissions increased steadily for two weeks in the flooded plots in V1 before they declined again (**Fig. S2b**, blue line). However, peaks in N_2O and CO_2 emissions following the flooding were not as high as the spike observed two months after flooding, shortly after both vineyards received 336 kg ha^{-1} of N fertilizer (ammonium sulfate 21-0-0 with 24% sulfur; end of Apr-2020), which was the only fertilizer application during that year. We note that CH_4 emissions were not detected during the experiments.

3.5. Yield data

Both vineyards were harvested in early Sep 2020. In V1, a significant 29% decrease in yield was observed compared to the control (t-test, $p < 0.05$), whereas in V2, there was no evidence of a significant difference in yield although yield was 14% lower in the flooded plots ($p = 0.24$) (**Fig. S3**).

4. Discussion

4.1. Nitrate leaching vs. denitrification during flooding

We observed a rapid decline in pore water NO_3^- concentrations within the first days of flooding for Ag-MAR. Two possible processes can be attributed to the observed NO_3^- decrease: NO_3^-

354 removal due to denitrification, a microbial-controlled process, and/or leaching of NO_3^-, a solute

355 transport process. The former would be preferable during Ag-MAR (or any other MAR type)

356 since it can transform NO_3^- into the inert gas N_2, thereby preventing NO_3^- from reaching the

357 groundwater (Levintal et al., 2022). Denitrification rates measured through incubation

358 experiments (Petersen et al., 2012; Verchot et al., 2001), showed the highest denitrification

359 activities in the top 0.1 m of the soil profile, decreasing to approximately zero below 0.6 m (**Fig.**

360 **S4**). Denitrification rates in the top 0.1 m were 1.4 and 1.35 mg NO_3^--N kg soil^{-1} d^{-1} for V1 and

361 V2, respectively. These rates are considered maximum rates, since they were obtained under

362 optimal conditions (25 °C, $O_2 \sim 0\%$, C substrate addition), favoring denitrification over

363 nitrification. In both vineyards, oxic conditions dominated the root zone before flooding started

364 and during imbibition. Thus, it is expected that denitrification rates were lower than the rates

365 derived from the incubation experiments, at least until the root zone became fully

366 suboxic/anoxic.

367 Infiltration rates not only determined the transition from oxic to suboxic conditions in each

368 vineyard, but also the rate at which NO_3^- was transported below the active denitrification zone in

369 the topsoil (i.e., 0-0.2 m). **Fig. 6** describes the tradeoff between the development of

370 suboxic/anoxic conditions and the depletion of NO_3^- at 0.2 m. To allow comparison between the

371 vineyards, NO_3^- concentrations in each vineyard were normalized to the initial concentrations

372 observed in each vineyard prior to flooding. V1 reached suboxic conditions at 0.2 m (ORP < 400

373 Eh) after one day of flooding, compared to V2 which developed suboxic conditions only after 10

374 days. When the transition from oxic to suboxic conditions occurred in V1, more than 80% of the

375 initial NO_3^- was still available at 0.2 m depth (**Fig. 6a,** blue squares). In contrast, by the time V2

376   reached suboxic conditions only ~10% of the initial NO_3^- was available for denitrification (**Fig.**

377   **6a,** red squares), indicating that 90% was leached.
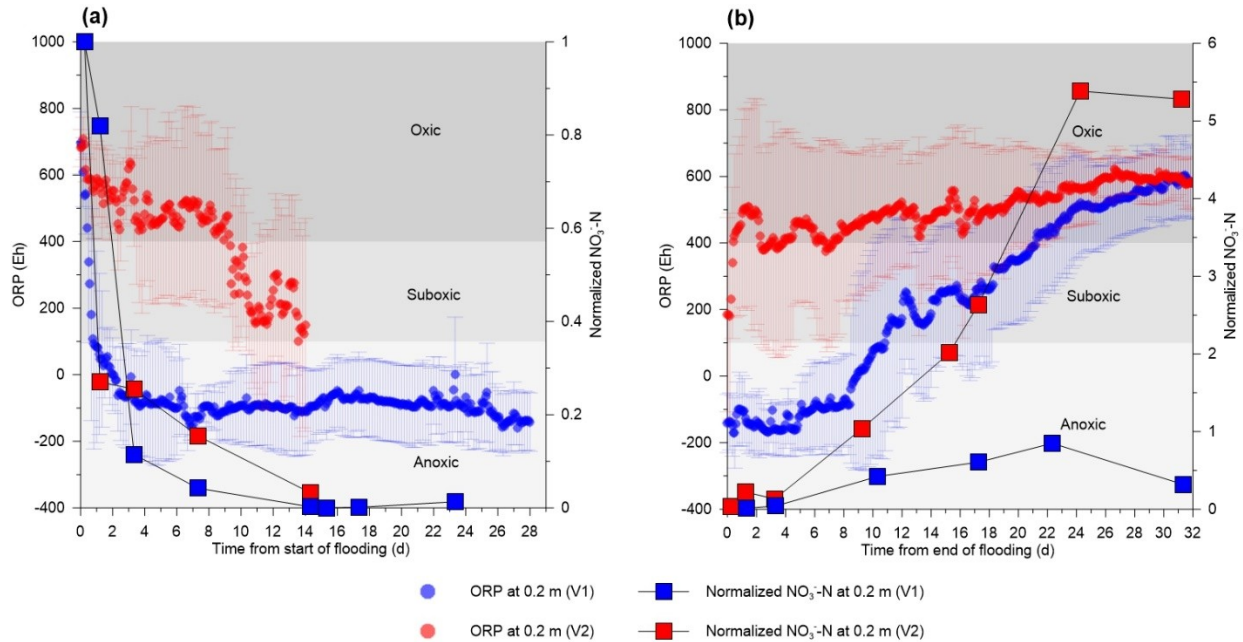
379   **Fig. 6**. Oxidation-reduction potential (ORP) and normalized pore water NO_3^- concentrations at

380   0.2 m depth during the wetting (a) and drying phase (b) of Ag-MAR. Values are averages of the

381   flooded profiles in each vineyard with error bars representing the standard deviation. NO_3^- was

382   normalized to the initial pore water NO_3^- concentrations in each vineyard; values above 1

383   indicate that NO_3^- exceeded the initial pre-flooding concentrations (i.e., V2 in subplot 'b').

384   The NO_3^- which was not consumed during the denitrification process in the topsoil was leached

385   below the root zone and eventually transported towards the groundwater as denitrification is

386   assumed to be negligible in the deep vadose zone (up to 3-5% per year) (Baram et al., 2016a). In

387   both vineyards, the majority of NO_3^- was leached below 1 m during the first week of flooding,

388   with a leaching peak of NO_3^- occurring during day 2 and 4 in V1 and V2, respectively (**Fig. 7a**).

389   The cumulative amount of NO_3^- leached (using **Eqs. 1** and **2**) was 10.3 and 1.6 g NO_3^--N m^{-2} for

390   V1 and V2, respectively (**Fig. 7b**), which equates to a NO_3^- loading of 47.4 and 4.3 kg NO_3^--N

391   for V1 (flooded area of 4,613 m^2) and V2 (flooded area of 3,035 m^2) below 1 m, respectively.

392   Averaging the cumulative NO_3^- leached per total applied water results in 8.6 and 1 g NO_3^--N m^{-2}

393   for every 1 cm^3 cm^{-2} of water applied for V1 and V2, respectively (i.e., an average leaching

394   concentration of 8.6 and 1 mg L^{-1} NO_3^--N for V1 and V2). These values are similar in magnitude

395   to NO_3^- leaching amounts estimated in a previous Ag-MAR field experiment (Bachand et al.,

396   2014) and in an Ag-MAR column experiment (Murphy et al., 2021). Yet, it is also possible to

397   have different leaching amounts between sites due to site-specific factors influencing nitrate

398   leaching (e.g., soil texture and soil pre-flooding NO_3^- concentration).
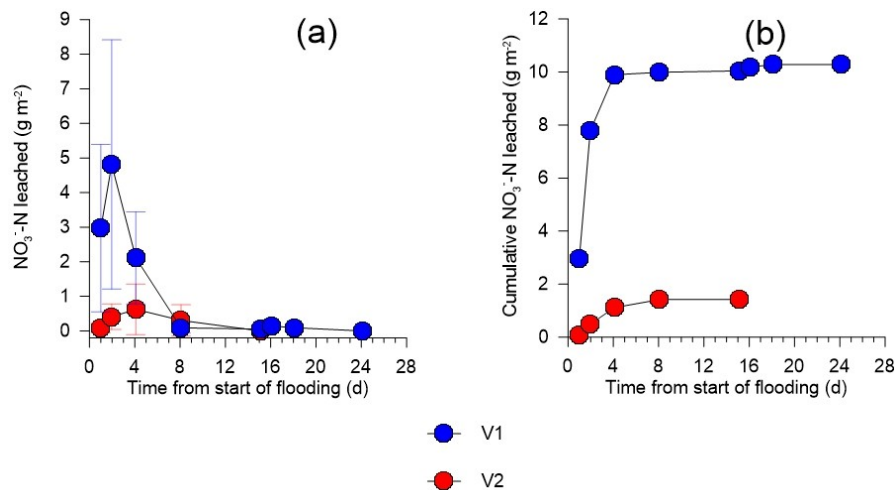
399

400   **Fig. 7**. Observed and cumulative amounts of NO_3^- leached below 1 m for (a) the 4-week flooded

401   vineyard (V1) and (b) the 2-week flooded vineyard (V2).

402   The amount of NO_3^- leached differed by one-order of magnitude between the two vineyards.

403   These differences can be attributed to the initial pore water and soil NO_3^- concentrations prior to

404   flooding. In V1, the pre-flooding pore water NO_3^- concentrations ranged between 20-80 mg NO_3^--

405   N L^{-1} (**Fig. 4b**), whereas in V2, concentrations were below 2 mg NO$_3^-$-N L^{-1} (**Fig. 4e**). Therefore,

406   estimating legacy NO$_3^-$ levels prior to Ag-MAR is essential for assessing leaching risks. It is

407   emphasized that the low initial NO$_3^-$ concentrations in V2's topsoil does not necessarily indicate

408   a lower risk of groundwater contamination. Both vineyards were fertilized and irrigated

409   following the same protocols in the years prior to the Ag-MAR experiment, and therefore, it is

410   likely that elevated NO$_3^-$ levels were also present in V2. Yet, the surplus NO$_3^-$ was pushed deeper

411   into the soil profile with each flood irrigation and precipitation event due to the higher infiltration

412   rate of V2 compared to V1.

413   Once pre-flooding pore water NO$_3^-$ depleted, concentrations in both vineyards and at all three

414   measured depths (0.2, 0.6, and 1 m) stayed zero for the remainder of the flooding even though

415   NO$_3^-$ was added to the system with the floodwater (2-3 mg NO$_3^-$-N L^{-1}; **Figs. 4b** and **e**, black

416   circles). The source water NO$_3^-$ was depleted by denitrification in the first 0.1 m of the soil

417   profile. This conclusion is supported by the denitrification rates estimated through lab incubation

418   experiments. For example, the denitrification rate estimated for the top 0.1 m soil profile in V1

419   was 1.4 mg NO$_3^-$-N kg soil^{-1} d^{-1} (**Fig. S4**), which translates to a potential *in-situ* soil

420   denitrification of 10 mg NO$_3^-$-N per day during flooding. This rate is ~5-fold higher than the

421   floodwater NO$_3^-$ concentration, thus can explain the NO$_3^-$ depletion during infiltration. At this

422   stage, water percolating below 1 m contributed to the dilution of the already leached residual soil

423   NO$_3^-$. This process is also refereed as the dilution effect (Bachand et al., 2014). While Ag-MAR

424   with low-contaminant water (e.g., rainfall-runoff or snowmelt) can cause not only NO$_3^-$ leaching

425   from the root zone, but also dilution of NO$_3^-$ in pore water, its final impact on groundwater

426   quality is a long-term process, which depends on several factors including the legacy NO$_3^-$ load

427   in the vadose zone, the NO_3^- concentration of groundwater, geogenic sources, and groundwater

428   flow velocity (Dahan et al., 2014; Levintal et al. 2022). Therefore, quantifying the dilution effect

429   from a single year is not feasible; further discussion is given below in section 4.3.

430   *4.2.   Post-flooding nitrogen dynamics*

431   Owing to the legacy of N in agricultural plant systems, we investigated the post-flooding N

432   cycling processes during the growing season. In V1, soil NH_4^+ levels recovered to pre-flooding

433   levels in the first two weeks after the flooding ended (**Fig. 5a**). An increase was also observed for

434   NO_3^-, however, only in the topsoil (**Fig. 5b**, 0-0.2 m). Similar post-flooding NH_4^+/NO_3^-

435   concentrations increases were observed in V2 (**Figs. 5c** and **5d**), while NH_4^+ increased at all

436   depths, NO_3^- increased only in the topsoil, indicating that mineralization occurred throughout the

437   1 m profile, whereas nitrification was mainly limited to the topsoil. NH_4^+ concentrations were an

438   order-of magnitude lower than NO_3^- for both pore water and soil. The accumulation of NO_3^- in

439   the top of the soil profile (0-0.2 m) rather than at deeper layers is consistent with previous studies

440   (e.g., Dahan et al., 2014) who concluded that this accumulation pattern is preferable for both

441   crop uptake and reducing leaching risks.

442   NO_3^- in pore water is considered to be more mobile in the vadose zone compared to the

443   immobile NH_4^+ cations attached to soil particles and organic matter (Subbarao and Searchinger,

444   2021). In terms of NO_3^- leaching risk, the chemical composition of the pore water has a more

445   immediate and significant effect on groundwater, rather than contaminants adsorbed onto

446   sediment in the immobile phase. Thus, prioritization of pore water data over soil data is

447   potentially recommended when assessing NO_3^- leaching risk to groundwater. We emphasize that

448   additional research is needed to validate this statement as previous studies also suggested that

449 nitrogen can be released from the soil to the pore water at later stages of the flooding and in the

450 deep vadose zone (Mienis and Arye, 2018; Xin et al., 2019). In general, the relationship between

451 pore water and soil samples is complex (Darrouzet-Nardi and Weintraub, 2014; Rimon et al.,

452 2011). Studies suggested equations to convert between the two (Zhu et al., 2021). Yet, to date, no

453 empirical relationship has been validated for different soils or soil moisture variations as

454 expected during flooding.

455 Anoxic conditions continued in V1 for about 3 weeks after the flooding ended, while V2 stayed

456 mostly in oxic conditions throughout and after the flooding (**Fig. 7b**). The topsoil (0.2 m) in V1's

457 flooded area stayed in anoxic/suboxic conditions for 20 consecutive days once flooding ended,

458 promoting denitrification. We observed elevated N_2O emissions, which can be a byproduct of

459 denitrification, in the 20 days of anoxic/suboxic conditions following the flooding of V1 (**Fig.**

460 **S2b**, blue circles during the start of April). We note that N_2O emissions can also be attributed to

461 nitrification, however, under near-saturated conditions denitrification dominates N_2O production

462 (Bateman and Baggs, 2005; Zhu et al., 2013). N_2O emissions started to decrease in V1 after the

463 20 days due to developing oxic conditions following flooding. N_2O emissions started to increase

464 again after the vineyard's fertilization and first irrigation of the growing season on 4/29/2021.

465 The measured N_2O emissions were similar in magnitude to reported fertilization-related

466 emissions from vineyards under a similar Mediterranean climate (Garland et al., 2014, 2011).

467 *4.3.   Conceptual model – coupling nitrogen and water dynamics under Ag-MAR*

468 We developed a conceptual model for N fate and transport in agricultural soils flooded for

469 extended periods of time with low-contaminant water for Ag-MAR (**Fig. 8**). The model was

470 developed based on data from the two vineyards investigated in this study and from recent Ag-

471   MAR studies conducted on alfalfa (Dahlke et al., 2018), almonds (Ganot and Dahlke, 2021b,

472   2021a), and in controlled soil column experiments (Murphy et al., 2021). We identify four stages

473   that determine N fate during Ag-MAR: pre-flooding, start of flooding, quasi-steady flooding, and

474   post-flooding. In each stage, the N fate is determined by the soil physico-chemical characteristics

475   and the initial N concentration.
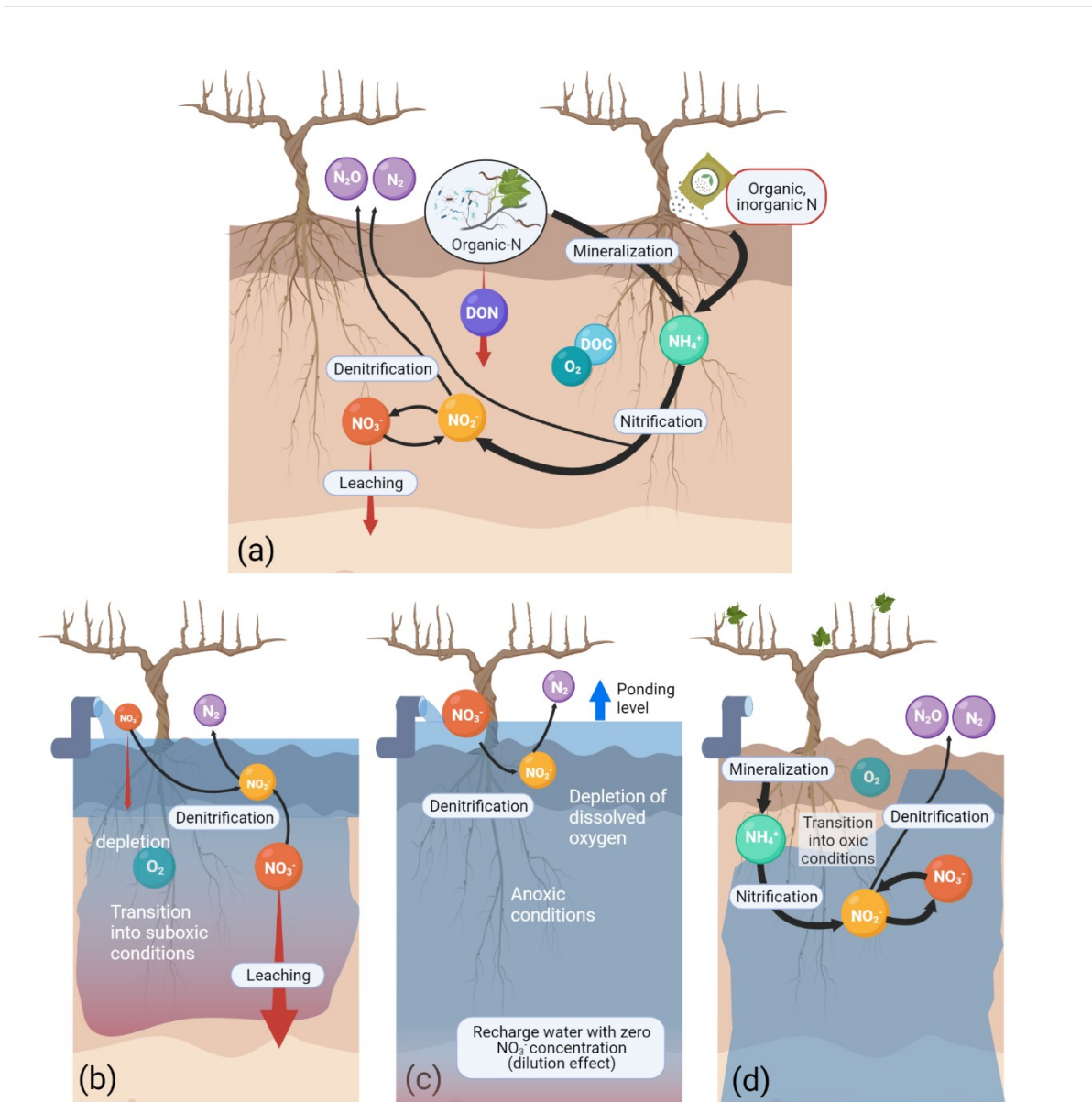
476

477 **Fig. 8**. Conceptual model for N fate under long-term flooding conditions at the topsoil. (a) pre-

478 flooding, (b) start of flooding, (c) quasi-steady flooding, and (d) post-flooding. Detailed

479 description for each stage is given in section 4.3. Figure created with Biorender.

480 *Pre-flooding stage:* In the pre-flooding stage (**Fig. 8a**), the root zone is unsaturated and

481 predominantly oxic. The soil matrix and pore water contain variable amounts of legacy inorganic

482 N species (i.e., NH_4^+ and NO_3^-) from previous fertilization events and from mineralization of

483 organic-N, which are either transported with the infiltrating water or transformed through various

484 microbial processes.

485 *Start of flooding stage:* With the start of flooding (**Fig. 8b**) the root zone saturates with water

486 thereby decreasing oxygen and ORP levels. This is the most dynamic stage during the flooding

487 event, yet with high environmental significance as this stage will define the magnitude of the

488 NO_3^- leached. The amount of NO_3^- leached below the root zone and the amount of NO_3^-

489 denitrified in the topsoil is dependent on site-specific physico-chemical parameters (K_{sat},

490 infiltration rate, ORP, available NO_3^- and carbon, and temperature) and the abundance and

491 activity of both nitrifying and denitrifying microbial communities in the topsoil. NO_3^- leaching is

492 the dominating loss process in soils with high K_{sat} (or infiltration rate), while denitrification plays

493 a larger role in soils with lower K_{sat} where the residence time of water in the topsoil is longer. Of

494 course, denitrification is the preferred loss pathway for NO_3^- to reduce NO_3^- contamination to

495 groundwater, however, in the time it takes to reach suboxic conditions that promote

496 denitrification, high K_{sat} soil might already leach > 80% of the legacy NO_3^- present in the profile.

497   *Quasi-steady flooding stage:* After the highly dynamic NO_3^- leaching and N transformation

498   phase at the start of flooding, the system transitions into the quasi-steady flooding stage (**Fig. 8c**),

499   which is characterized by saturated, suboxic/anoxic conditions and more stable soil physico-

500   chemical parameters. If anoxic conditions are reached in the root zone, it can be assumed that

501   dissolved oxygen is likewise depleted as reported in other MAR studies (Turkeltaub et al., 2022).

502   Under these conditions, denitrifiers in the topsoil consume NO_3^- in the infiltrating water. This

503   NO_3^- removal will eventually contribute to the dilution of pore water NO_3^- in the vadose zone.

504   Sustaining the quasi-steady flooding stage for as long as possible is preferred because it increases

505   the amount of 'clean' recharge while reducing NO_3^- levels in the pore water transported to

506   groundwater. However, the dilution effect only takes effect if NO_3^- concentrations in the source

507   water are relatively low and the retention time of the infiltrating water in the denitrifying soil

508   layer is sufficiently long to allow complete NO_3^- consumption. For example, in this study,

509   infiltration rates of 0.1-0.2 m d^{-1} were sufficient to allow denitrification of NO_3^- in the source

510   water (2-3 mg NO_3^--N L^{-1}) in the first 0.2 m of the soil profile. If recharge water is sourced from

511   pristine streamflow, it is typically low in NO_3^- concentrations. Hence, there is a high probability

512   for the dilution effect to occur during the quasi-steady flooding stage when implementing Ag-

513   MAR for periods of more than several days. However, flooding fields for long periods of time

514   might negatively impact crop performance, as shown for V1, which needs to be considered and

515   balanced (Levintal et al., 2022). A possible solution is to use a new model that predicts crop

516   damage as a function of the duration of saturated conditions in the soil root-zone, soil texture,

517   and crop tolerance to waterlogged conditions (Ganot and Dahlke, 2021a).

518 *Post-flooding stage:* In the post-flooding stage (**Fig. 8d**), oxygen and ORP will gradually

519 increase back to pre-flooding oxic levels. In soils with higher infiltration rates (sand or loamy-

520 sand) this process can take several days compared to several weeks in soils with lower

521 infiltration rates (e.g., sandy loam or loam). Soil moisture will also decrease from near- or full-

522 saturation to pre-flooding levels. However, this process is relatively slow (on the scale of weeks

523 to months) and controlled also by precipitation or irrigation events that will temporarily increase

524 soil moisture in the root zone. A post-flooding increase in NO_3^- and NH_4^+ is also expected,

525 mainly in the topsoil (0-0.2 m) as a result of mineralization and nitrification. Denitrification is

526 another post-flooding process that can occur, yet it will be more pronounced in soils with slow

527 infiltration rates when soil moisture is still high during the first stage of drainage when

528 anoxic/suboxic conditions prevail (V1 in this study).

529 Ag-MAR includes three distinct differences compared to other MAR types (Goren et al., 2014;

530 Gorski et al., 2020, 2019; Mienis and Arye, 2018): (1) the nitrogen source is mainly in the soil

531 rather than in the recharge water, (2) recharge (i.e., the flooding) will be primarily seasonal

532 during wet periods and not yearly with continuous flooding and drying cycles, and (3) the

533 infiltration basin is not necessarily on high-infiltrating land, such as sandy soil. Therefore,

534 caution should be taken when adapting the four model's stages for long-term flooding of other

535 MAR types. For example, nitrogen fate under soil aquifer treatment (SAT; a MAR form where

536 treated wastewater is recharged) showed highly complex biogeochemical processes due to

537 changing nitrogen and carbon loading (e.g. NH_4^+) in the source water (Mienis and Arye, 2018).

538 This resulted in varying nitrate concentrations in the groundwater during the recharge, which our

539 model cannot adequately explain.

4.4.   Implications for Ag-MAR operation

540

541   Understanding the N-related dynamics at each stage of Ag-MAR as presented in the conceptual

542   model (**Fig. 8**) is essential for the development of best management practices. Taking V1 as a

543   case study, a better practice to decrease the risk of NO_3^- leaching would be to irrigate the

544   vineyard initially for 1-2 days (before the continuous flooding for Ag-MAR) until anoxic

545   conditions are developed, which would promote denitrification and minimize NO_3^- leaching.

546   Maintaining anoxic conditions is also important for the inhibition of the nitrification process that

547   can increase inorganic NO_3^- concentrations between individual recharge (i.e., flooding) events.

548   The predicted outcome of the suggested recharge practice will be a decrease in the overall

549   amount of NO_3^- leached. However, this practice is unlikely to be applicable in high infiltrating

550   soils in which nearly all the initial NO_3^- will be leached in the first few days before the

551   development of anoxic conditions (V2 in this study, infiltration rate of 0.171 m d^{-1}). A more

552   detailed discussion on the trade-offs between leaching and mineralization–denitrification

553   processes under repeated flooding events is provided by Murphy et al. (2021).

554   Our study was conducted in a Mediterranean climate, and therefore, adjustments are needed if

555   adapting the findings to other locations. For instance, lower ambient soil temperatures will

556   decrease the rate at which nitrification/denitrification occurs and to a lesser extent also influence

557   the infiltration rate (Grinshpan et al., 2022). Thus, Ag-MAR implementation in colder climates

558   will decrease denitrification rates during infiltration, potentially increasing the risk for leaching

559   of soil residual NO_3^-. Other considerations for Ag-MAR implementation are non-point source

560   contaminants with high leaching risks, such as salts, pesticides, and inorganic geogenic

561   contaminates. A comprehensive review of these contaminants with potential solutions is

33

562　provided in Levintal et al. (2022). Still, high NO_3^- concentration in the aquifer is the main

563　concern at global scale (Beganskas et al., 2018; Dahan et al., 2014). With respect to yield,

564　several reasons can explain the yield difference between the vineyards investigated in this study,

565　such as differences in soil texture and the resulting K_{sat}, infiltration rates, O_2/redox levels,

566　duration of flooding, movement of available N below root zone, and timing of flooding with

567　respect to bud break in March. Therefore, possible effects on yield should be investigated in

568　more detail, and until then, caution is advised in using Ag-MAR in late winter-early spring, in

569　vineyards with less-than-ideal soil properties.

570　**5.　Conclusions**

571　 An agricultural managed aquifer recharge (Ag-MAR) experiment was conducted in the Central

572　Valley of California on two vineyards managed similarly but differing in soil texture and

573　hydraulic properties. One vineyard was flooded for four weeks (V1) and the other for two weeks

574　(V2). Although the flooding for groundwater recharge started on the same day, different soil

575　biogeochemical outcomes occurred. Suboxic conditions, favoring denitrification in the

576　microbially active topsoil (0-0.2 m), developed in the vineyard with the low-infiltration rate

577　(0.088 m d^{-1}; V1) in less than one day, compared to 10 days in the high-infiltration vineyard

578　(0.171 m d^{-1}; V2). Nevertheless, in both vineyards, NO_3^- leaching was the dominant N loss

579　process while denitrification played a lesser role in decreasing NO_3^- in the root zone. The amount

580　of NO_3^- leached below the 1 m root zone was mainly determined by the amount of residual NO_3^-

581　present in the root zone prior to the flooding for groundwater recharge, showcasing the

582　importance of estimating legacy NO_3^- pools before establishing an Ag-MAR site.

583　　A conceptual model for water-N dynamics under Ag-MAR was developed based on hydrologic,

584　　geochemical, and microbial process analyses. Four stages were identified: pre-flooding, start of

585　　flooding, quasi-steady flooding, and post-flooding. Out of the above, the start of flooding is the

586　　most dynamic stage that will define the magnitude of NO_3^- leached. The proposed model can be

587　　used to determine best Ag-MAR management practices. Adoption of Ag-MAR, as one approach

588　　in a portfolio of MAR methods, is desirable as population growth and expansion of irrigated

589　　agriculture contribute to unsustainable groundwater extraction and a growing need to replenish

590　　groundwater resources to buffer growing water supply variability.

CRediT authorship contribution statement

Elad Levintal: Methodology, Writing – original draft, Formal analysis. **Laibin Huang:** Writing - review& editing, Formal analysis. **Cristina Prieto García:** Methodology, Writing - review& editing, Formal analysis. **Adolfo Coyotl:** Writing - review& editing, Formal analysis. **Matthew W. Fidelibus:** Writing - review& editing, Formal analysis. **William R. Horwath:** Writing - review& editing, Funding acquisition. **Jorge L. Mazza Rodrigues:** Writing - review& editing, Funding acquisition. **Helen E. Dahlke:** Supervision, Methodology, Writing - review& editing, Funding acquisition.

Declaration of competing interest

The authors declare that they have no known competing financial interests or personal relationships that could have appeared to influence the work reported in this paper.

Acknowledgments

36

References

609

610 Araujo, F., Williams, L.E., Grimes, D.W., Matthews, M.A., 1995. A comparative study of young

611   "Thompson Seedless" grapevines under drip and furrow irrigation. I. Root and soil water

612   distributions. Sci. Hortic. (Amsterdam). 60, 235–249.

613 Bachand, P.A.M., Roy, S.B., Choperena, J., Cameron, D., Horwath, W.R., 2014. Implications of

614   using on-farm flood flow capture to recharge groundwater and mitigate flood risks along the

615   Kings River, CA. Environ. Sci. Technol. 48, 13601–13609.

616 Baram, S., Couvreur, V., Harter, T., Read, M., Brown, P.H., Hopmans, J.W., Smart, D.R., 2016a.

617   Assessment of orchard N losses to groundwater with a vadose zone monitoring network.

618   Agric. Water Manag. 172, 83–95.

619 Baram, S., Couvreur, V., Harter, T., Read, M., Brown, P.H., Kandelous, M., Smart, D.R.,

620   Hopmans, J.W., 2016b. Estimating nitrate leaching to groundwater from orchards:

621   Comparing crop nitrogen excess, deep vadose zone sata-sriven estimates, and HYDRUS

622   modeling. Vadose Zo. J. 15, 1–13.

623 Bateman, E.J., Baggs, E.M., 2005. Contributions of nitrification and denitrification to N2O

624   emissions from soils at different water-filled pore space. Biol. Fertil. Soils 41, 379–388.

625 Beganskas, S., Gorski, G., Weathers, T., Fisher, A.T., Schmidt, C., Saltikov, C., Redford, K.,

626   Stoneburner, B., Harmon, R., Weir, W., 2018. A horizontal permeable reactive barrier

627   stimulates nitrate removal and shifts microbial ecology during rapid infiltration for managed

628   recharge. Water Res. 144, 274–284.

629 Bishayee, B., Chatterjee, R.P., Ruj, B., Chakrabortty, S., Nayak, J., 2022. Strategic management

630   of nitrate pollution from contaminated water using viable adsorbents: An economic

631   assessment-based review with possible policy suggestions. J. Environ. Manage. 303,

632   114081.

633 Connor, R., 2015. The United Nations world water development report 2015: Water for a

634   sustainable world. UNESCO publishing, Paris.

635 Dahan, O., Babad, A., Lazarovitch, N., Russak, E.E., Kurtzman, D., 2014. Nitrate leaching from

636   intensive organic farms to groundwater. Hydrol. Earth Syst. Sci. 18, 333–341.

637 Dahlke, H.E., Brown, A.G., Orloff, S., Putnam, D., O'Geen, T., 2018. Managed winter flooding

638   of alfalfa recharges groundwater with minimal crop damage. Calif. Agric. 72, 65–75.

639 Darrouzet-Nardi, A., Weintraub, M.N., 2014. Evidence for spatially inaccessible labile N from a

640   comparison of soil core extractions and soil pore water lysimetry. Soil Biol. Biochem. 73,

641   22–32.

642 Dillon, P., Stuyfzand, P., Grischek, T., Lluria, M., Pyne, R.D.G., Jain, R.C., Bear, J., Schwarz, J.,

643   Wang, W., Fernandez, E., Stefan, C., Pettenati, M., van der Gun, J., Sprenger, C.,

644   Massmann, G., Scanlon, B.R., Xanke, J., Jokela, P., Zheng, Y., Rossetto, R., Shamrukh, M.,

645   Pavelic, P., Murray, E., Ross, A., Bonilla Valverde, J.P., Palma Nava, A., Ansems, N.,

646   Posavec, K., Ha, K., Martin, R., Sapiano, M., 2019. Sixty years of global progress in

647   managed aquifer recharge. Hydrogeol. J. 27, 1–30.

648 Ganot, Y., Dahlke, H.E., 2021a. A model for estimating Ag-MAR flooding duration based on

649   crop tolerance, root depth, and soil texture data. Agric. Water Manag. 255, 107031.

650   Ganot, Y., Dahlke, H.E., 2021b. Natural and forced soil aeration during agricultural managed

651   aquifer recharge. Vadose Zo. J. 20, 1–19.

652   Garland, G.M., Suddick, E., Burger, M., Horwath, W.R., Six, J., 2014. Direct N2O emissions

653   from a Mediterranean vineyard: Event-related baseline measurements. Agric. Ecosyst.

654   Environ. 195, 44–52.

655   Garland, G.M., Suddick, E., Burger, M., Horwath, W.R., Six, J., 2011. Direct N2O emissions

656   following transition from conventional till to no-till in a cover cropped Mediterranean

657   vineyard (Vitis vinifera). Agric. Ecosyst. Environ. 141, 234–239.

658   Gorelick, S.M., Zheng, C., 2015. Global change and the groundwater management challenge.

659   Water Resour. Res. 51, 3031–3051.

660   Goren, O., Burg, A., Gavrieli, I., Negev, I., Guttman, J., Kraitzer, T., Kloppmann, W., Lazar, B.,

661   2014. Biogeochemical processes in infiltration basins and their impact on the recharging

662   effluent, the soil aquifer treatment (SAT) system of the Shafdan plant, Israel. Appl.

663   Geochemistry 48, 58–69.

664   Gorski, G., Dailey, H., Fisher, A.T., Schrad, N., Saltikov, C., 2020. Denitrification during

665   infiltration for managed aquifer recharge: Infiltration rate controls and microbial response.

666   Sci. Total Environ. 727.

667   Gorski, G., Fisher, A.T., Beganskas, S., Weir, W.B., Redford, K., Schmidt, C., Saltikov, C.,

668   2019. Field and laboratory studies linking hydrologic, geochemical, and microbiological

669   processes and enhanced denitrification during infiltration for managed recharge. Environ.

670   Sci. Technol. 53, 9491–9501.

671   Grinshpan, M., Furman, A., Dahlke, H.E., Raveh, E., Weisbrod, N., 2021. From managed aquifer

672   recharge to soil aquifer treatment on agricultural soils: concepts and challenges. Agric.

673   Water Manag. 255, 106991.

674   Grinshpan, M., Turkeltaub, T., Furman, A., Raveh, E., Weisbrod, N., 2022. On the use of

675   orchards to support soil aquifer treatment systems. Agric. Water Manag. 260, 107315.

676   Gurevich, H., Baram, S., Harter, T., 2021. Measuring nitrate leaching across the critical zone at

677   the field to farm scale. Vadose Zo. J. 1–16.

678   Haddeland, I., Heinke, J., Biemans, H., Eisner, S., Flörke, M., Hanasaki, N., Konzmann, M.,

679   Ludwig, F., Masaki, Y., Schewe, J., Stacke, T., Tessler, Z.D., Wada, Y., Wisser, D., 2014.

680   Global water resources affected by human interventions and climate change. Proc. Natl.

681   Acad. Sci. U. S. A. 111, 3251–3256.

682   Kocis, T.N., Dahlke, H.E., 2017. Availability of high-magnitude streamflow for groundwater

683   banking in the Central Valley, California. Environ. Res. Lett. 12.

684   Kraft, B., Tegetmeyer, H.E., Sharma, R., Klotz, M.G., Ferdelman, T.G., Hettich, R.L., Geelhoed,

685   J.S., Strous, M., 2014. The environmental controls that govern the end product of bacterial

686   nitrate respiration. Science (80-.). 345, 676–679.

687   Kurtzman, D., Kanner, B., Levy, Y., Nitsan, I., Bar-Tal, A., 2021. Maintaining intensive

688   agriculture overlying aquifers using the threshold nitrate root-uptake phenomenon. J.

689   Environ. Qual. 1–11.

690 Levintal, E., Kniffin, M.L., Ganot, Y., Marwaha, N., Murphy, N.P., Dahlke, H.E., 2022.

691   Agricultural managed aquifer recharge (Ag-MAR)—a method for sustainable groundwater

692   management: A review. Crit. Rev. Environ. Sci. Technol. 0, 1–24.

693 Long, A., Heitman, J., Tobias, C., Philips, R., Song, B., 2013. Co-occurring anammox,

694   denitrification, and codenitrification in agricultural soils. Appl. Environ. Microbiol. 79,

695   168–176.

696 Mienis, O., Arye, G., 2018. Long-term nitrogen behavior under treated wastewater infiltration

697   basins in a soil-aquifer treatment (SAT) system. Water Res. 134, 192–199.

698 Murphy, N.P., Waterhouse, H., Dahlke, H.E., 2021. Influence of agricultural managed aquifer

699   recharge on nitrate transport: The role of soil texture and flooding frequency. Vadose Zo. J.

700   20, 1–16.

701 Negri, C., Chiaradia, E., Rienzner, M., Mayer, A., Gandolfi, C., Romani, M., Facchi, A., 2020.

702   On the effects of winter flooding on the hydrological balance of rice areas in northern Italy.

703   J. Hydrol. 590, 125401.

704 Niswonger, R.G., Morway, E.D., Triana, E., Huntington, J.L., 2017. Managed aquifer recharge

705   through off-season irrigation in agricultural regions. Water Resour. Res. 53, 6970–6992.

706 O'Geen, A.T., Saal, M., Dahlke, H., Doll, D., Elkins, R., Fulton, A., Fogg, G., Harter, T.,

707   Hopmans, J.W., Ingels, C., Niederholzer, F., Solis, S.S., Verdegaal, P., Walkinshaw, M.,

708   2015. Soil suitability index identifies potential areas for groundwater banking on

709 agricultural lands. Calif. Agric. 69, 75–84.

710 Onsoy, Y.S., Harter, T., Ginn, T.R., Horwath, W.R., 2005. Spatial Variability and Transport of

711 Nitrate in a Deep Alluvial Vadose Zone. Vadose Zo. J. 4, 41–54.

712 Owens, P.R., Wilding, L.P., Lee, L.M., Herbert, B.E., 2005. Evaluation of platinum electrodes

713 and three electrode potential standards to determine electrode quality. Soil Sci. Soc. Am. J.

714 69, 1541–1550.

715 Petersen, D.G., Blazewicz, S.J., Firestone, M., Herman, D.J., Turetsky, M., Waldrop, M., 2012.

716 Abundance of microbial genes associated with nitrogen cycling as indices of

717 biogeochemical process rates across a vegetation gradient in Alaska. Environ. Microbiol.

718 14, 993–1008.

719 Peterson, M.E., Curtin, D., Thomas, S., Clough, T.J., Meenken, E.D., 2013. Denitrification in

720 vadose zone material amended with dissolved organic matter from topsoil and subsoil. Soil

721 Biol. Biochem. 61, 96–104.

722 Richa, A., Touil, S., Fizir, M., 2022. Recent advances in the source identification and

723 remediation techniques of nitrate contaminated groundwater: A review. J. Environ. Manage.

724 316, 115265.

725 Rimon, Y., Nativ, R., Dahan, O., 2011. Physical and Chemical Evidence for Pore-Scale Dual-

726 Domain Flow in the Vadose Zone. Vadose Zo. J. 10, 322–331.

727 Scarlett, K., Denman, S., Clark, D.R., Forster, J., Vanguelova, E., Brown, N., Whitby, C., 2021.

728 Relationships between nitrogen cycling microbial community abundance and composition

729   reveal the indirect effect of soil pH on oak decline. ISME J. 15, 623–635.

730   Schmidt, C.M., Fisher, A.T., Racz, A., Wheat, C.G., Los Huertos, M., Lockwood, B., 2012.

731   Rapid nutrient load reduction during infiltration of managed aquifer recharge in an

732   agricultural groundwater basin: Pajaro Valley, California. Hydrol. Process. 26, 2235–2247.

733   Schmidt, C.M., Fisher, A.T., Racz, A.J., Lockwood, B.S., Huertos, M.L., 2011. Linking

734   denitrification and infiltration rates during managed groundwater recharge. Environ. Sci.

735   Technol. 45, 9634–9640.

736   Siebert, S., Burke, J., Faures, J.M., Frenken, K., Hoogeveen, J., Döll, P., Portmann, F.T., 2010.

737   Groundwater use for irrigation - A global inventory. Hydrol. Earth Syst. Sci. 14, 1863–

738   1880.

739   Steenhuis, T., Molen, W., 1986. The TM procedure as a simple engineering method to predict

740   recharge. J. Hydrol. 84, 221–229.

741   Stein, L.Y., Klotz, M.G., 2016. The nitrogen cycle. Curr. Biol. 26, R94–R98.

742   Subbarao, G. V., Searchinger, T.D., 2021. A "more ammonium solution" to mitigate nitrogen

743   pollution and boost crop yields. Proc. Natl. Acad. Sci. U. S. A. 118, 1–5.

744   Turkeltaub, T., Furman, A., Mannheim, R., Weisbrod, N., 2022. Continuous monitoring of a soil

745   aquifer treatment system's physico-chemical conditions to optimize operational

746   performance. Hydrol. Earth Syst. Sci. 26, 1565–1578.

747   Van Meter, K.J., Basu, N.B., Veenstra, J.J., Burras, C.L., 2016. The nitrogen legacy: Emerging

748   evidence of nitrogen accumulation in anthropogenic landscapes. Environ. Res. Lett. 11.

43

749   Verchot, L. V., Holmes, Z., Mulon, L., Groffman, P.M., Lovett, G.M., 2001. Gross vs net rates

750   of N mineralization and nitrification as indicators of functional differences between forest

751   types. Soil Biol. Biochem. 33, 1889–1901.

752   Wada, Y., Van Beek, L.P.H., Van Kempen, C.M., Reckman, J.W.T.M., Vasak, S., Bierkens,

753   M.F.P., 2010. Global depletion of groundwater resources. Geophys. Res. Lett. 37, 1–5.

754   Waterhouse, H., Arora, B., Spycher, N.F., Nico, P.S., Ulrich, C., Dahlke, H.E., Horwath, W.R.,

755   2021. Influence of Agricultural Managed Aquifer Recharge (AgMAR) and Stratigraphic

756   Heterogeneities on Nitrate Reduction in the Deep Subsurface. Water Resour. Res. 57, 1–22.

757   Waterhouse, H., Bachand, S., Mountjoy, D., Choperena, J., Bachand, P.A.M., Dahlke, H.E.,

758   Horwath, W.R., 2020. Agricultural managed aquifer recharge - water quality factors to

759   consider. Calif. Agric. 74, 144–154.

760   Weitzman, J.N., Brooks, J.R., Compton, J.E., Faulkner, B.R., Mayer, P.M., Peachey, R.E., Rugh,

761   W.D., Coulombe, R.A., Hatteberg, B., Hutchins, S.R., 2022. Deep soil nitrogen storage

762   slows nitrate leaching through the vadose zone. Agric. Ecosyst. Environ. 332, 107949.

763   Xin, J., Liu, Y., Chen, F., Duan, Y., Wei, G., Zheng, X., Li, M., 2019. The missing nitrogen

764   pieces: A critical review on the distribution, transformation, and budget of nitrogen in the

765   vadose zone-groundwater system. Water Res. 165, 114977.

766   Zhang, Y., Ding, H., Zheng, X., Cai, Z., Misselbrook, T., Carswell, A., Müller, C., Zhang, J.,

767   2018. Soil N transformation mechanisms can effectively conserve N in soil under saturated

768   conditions compared to unsaturated conditions in subtropical China. Biol. Fertil. Soils 54,

769   495–507.

770   Zhu, X., Burger, M., Doane, T.A., Horwath, W.R., 2013. Ammonia oxidation pathways and

771   nitrifier denitrification are significant sources of N2O and NO under low oxygen

772   availability. Proc. Natl. Acad. Sci. U. S. A. 110, 6328–6333.

773   Zhu, Y., Chen, Y., Ali, M.A., Dong, L., Wang, X., Archontoulis, S. V., Schnable, J.C.,

774   Castellano, M.J., 2021. Continuous in situ soil nitrate sensors: The importance of high-

775   resolution measurements across time and a comparison with salt extraction-based methods.

776   Soil Sci. Soc. Am. J. 85, 677–690.

777